Journal of Minerals and Materials Characterization and Engineering, 2026, 14(3), 81-107
https://www.scirp.org/journal/jmmce
ISSN Online: 2327-4085
ISSN Print: 2327-4077

Study of the Production and Characterization of the Physicochemical and Mechanical Properties of a Wood-Kaolin Composite: Case of the Tropical Wood Species Ayous

Armonic Harold Noubissi Fonkwa[1], Cyrille Ghislin Fotsop[2], Roland Urselin Noumsi Foko[3], Paul Alain Nanssou Kouteu[1], Thomas Djiako[4,5], Donald Raoul Tchuifon Tchuifon[1*]

[1]Department of Process Engineering, Laboratory of Chemical Engineering and Industrial Bioprocesses, National Polytechnic School of Douala, University of Douala, Douala, Cameroon
[2]Institute of Chemistry, Faculty of Process and Systems Engineering, University Splatz 2, Magdeburg, Germany
[3]Department of Chemistry, Faculty of Sciences, University of Douala, Douala, Cameroon
[4]Department of Energy and Mechanical Engineering, ISTA-IUG, University of Ngaoundere, Ngaoundere, Cameroon
[5]Gulf of Guinea University Institute/ISTA, Douala, Cameroon
Email: *tchuifondonald@yahoo.fr

How to cite this paper: Fonkwa, N.A.H., Fotsop, C.G., Foko, N.R.U, Kouteu, N.P.A., Djiako, T. and Tchuifon, T.D.R (2026) Study of the Production and Characterization of the Physicochemical and Mechanical Properties of a Wood-Kaolin Composite: Case of the Tropical Wood Species Ayous. *Journal of Minerals and Materials Characterization and Engineering*, **14**, 81-107.
https://doi.org/10.4236/jmmce.2026.143007

Received: March 16, 2026
Accepted: May 26, 2026
Published: May 29, 2026

Abstract

This research highlights a non-exhaustive study of the production and characterization of the physico-chemical and mechanical properties of a unique wood-kaolin composite. XRD, FT-IR, and SEM-EDX analyses reveal that the clay composition is dominated by quartz and kaolinite, with particles arranged on either side in different shapes. The peaks present on the diffractogram of ayous wood sawdust are associated with planes attributed to the crystallographic plane of cellulose and show small fibers (microfibrils) that are generally made of cellulose and lignin, which make up the main component of the wood. As for the mechanical characterization, the panels PC (225.13 MPa), PB (189.53 MPa), and PH (182.83 MPa) exhibit the highest yield limits. The PH (269.46 MPa), PC (254.93 MPa), and PA (254.76 MPa) panels show the highest maximum strengths. The PH specimen (24.36 MPa) has the best ability to resist bending while maintaining its stiffness. Conversely, the PD specimen (15.70 MPa) has the lowest Young's modulus.

Keywords

Composite, Physicochemical and Mechanical Properties, Wood, Clay

1. Introduction

Developing countries produce a considerable amount of waste from the wood processing industry. Upstream forestry production, as well as the wood processing industries, feel this imbalance in the utilization of machining residues [1]. Only 30 to 36% of wood volumes are processed in Cameroon due to poor industrial performance in wood processing; about 64 to 70% of the wood ends up as residues in sawmills, and only 10% of sawmill residues are utilized [2]. This will lead to a wood shortage according to figures provided by WWF Brazil (2014). It is estimated that the global annual demand for wood is expected to increase from 6 to 8 billion m^3 by 2050 [3]. The residues from wood processing in Cameroon lack awareness of environmentally responsible valorization; most of the population uses these waste materials in the poultry sector for sanitation, as energy sources, while others are left abandoned. These resources, whether exploited or underutilized and available in nature, can contribute to the production of various materials useful to the public [2] [4]. Reducing greenhouse gas emissions and the carbon footprint worldwide remains a priority in preserving renewable resources; the creation and modernization of products from biomass as basic materials should remain a priority for actors in the forestry and wood industries [5]. This brings us to look into the valorization of wood residues known in Cameroon, Gabon, and Congo under the name Ayous (*Triplochiton scleroxylon*). Its valorization in our study is due to the fact that Ayous, like other white woods, is classified among second-choice species on the market in terms of quality and reduced physical and mechanical resistance. However, its wide geographical distribution and great availability remain an exception. The large diameter of the logs and the size of Ayous wood make it economically viable [6]. This study focuses on an innovative area involving the combination of two materials, wood and clay, to make a composite panel. The combination of diverse materials results in the formulation of a solid, multi-phase composite material, consisting of at least two immiscible materials with complementary characteristics [7]. Having a variety of structural and non-structural applications for both indoor and outdoor purposes, such as furniture, structural elements, flooring, windows, or doors, they have many applications in construction [8]. This is the case for panels reinforced with synthetic and natural fibers found on the market. Moreover, low density, non-toxicity, and a non-abrasive nature for equipment are the characteristics of a composite material reinforced with natural fiber; it differs from one reinforced with fiberglass [7]. The greatest challenge faced by panel manufacturing industries is the presence of unwanted foreign substances in the residues. Indeed, one of the two major components of the panel, apart from the wood fibers, is urea-formaldehyde resin or Phenol-formaldehyde. The methanol present in the resin is harmful to human health and can cause damage when these residues are reused in the environment [9] [10]. Several studies have explored similar avenues, Gwon *et al.* (2012) [11] worked on the development of a composite made from wood-plastic hybridized with inorganic fillers. Subsequently, the study of the production and characterization of

wood-plastic composites was addressed by Mahfoudh (2013) [7]. The development of an ultra-lightweight thermal insulation panel based on expanded perlite (Çelik and Durmuş, 2022) [12], as well as insulating structural composite panels made of glass fiber-reinforced polymer and cement-based materials Peng *et al.* (2021) [13], were studied. The use of kaolin and fibers for the manufacture of thermal insulation panels was studied by Reddy *et al.* (2024) [14]. Although prior studies have investigated the incorporation of mineral fillers or natural fibers into composites based on harmful adhesives, their application to particleboard manufacturing remains limited. The originality of the present study lies in the formulation of a structural composite panel combining exclusively machining residues from Ayous (*Triplochiton scleroxylon*) and a natural clay matrix, all stabilized with a health-friendly vinyl binder.

This raises the interest of our research on wood-clay composites optimized using an experimental design, representing an emerging class of hybrid materials that combines the advantages of natural wood with the characteristics of clay. This composite panel thus offers wide applications in various industrial sectors. Once again, this innovative blend of renewable raw materials and minerals is generating growing interest in meeting the sustainability and performance requirements of modern materials.

In this context, the study presented offers a thorough analysis of the production and characterization of the physicochemical and mechanical properties of this unique composite, in order to shed light on its feasibility and potential applications in indoor and outdoor furniture.

2. Materials and Methods

2.1. Material

The materials and devices that were used for this work are as follows: Sieve; a pH meter with a temperature probe; an electronic scale; a pair of gloves; a container for the mixtures; a release agent (cling film); vinyl adhesive wood purchased from the SONECO supermarket located in Bastos, in the Yaoundé 1 district, Mfoundi department, Central Region of Cameroon. An oven; a sprayer; a mixer: located within the Laboratory of Chemical Engineering and Industrial Bioprocesses at the University of Douala. A grinder: located at the Congo Market in Douala II and suited to our type of work. A mold: designed and manufactured taking into account the standards of the various tests to be carried out.

2.2. Basic Constituent Materials

The production of the composite panel was carried out using wood particles of ayous (Triplochiton chleroxylon) sourced from a sawmill in Bondje, located in the East of Cameroon, in the Boumba and Ngoko department, Yokadouma district. The granulometric selection of the Ayous wood particles was based on previous work, using a sieve size between (0.31 - 0.35 µm), which yielded satisfactory results [1] [2]. The clay matrix was collected in Mbalmayo near the Nyong River in the

Nyong and So'o department, Central region of Cameroon. The water-based white vinyl glue additive, suitable for all types of wood [15], was purchased from a supermarket in the center region. The wood sawdust and clay were air-dried in the sun before being placed in an oven at 103 ± 2˚C until reaching an anhydrous state, in order to stabilize them (sample mass fluctuating below 0.1% successively between two weightings within a 2-hour interval). **Figure 1** and **Figure 2** below show the steps for obtaining wood and clay particles.

2.3. Method for Preparing Wood Sawdust and Clay Materials

2.3.1. Preparation of Ayous Wood Sawdust

The process of preparing Ayous wood sawdust is carried out through a long process as shown in (**Figure 1(a)** & **Figure 1(b)**), in order to remove all impurities and improve its properties through its particle size [16].

Figure 1. (a) Diagram of the Ayous sawdust preparation process; (b) Preparation of Ayous sawdust.

The procedure below (**Figure 1(b)**) involves collecting the wood, cutting it, grinding it, drying it, and sieving it; this sieving allows for obtaining wood particles suitable for physico-chemical characterization.

Ayous wood sawdust naturally contains moisture, which can affect the properties of the composite when it is incorporated. By drying the wood sawdust, part of this moisture is being reduced. After harvesting, the wood was fragmented into small pieces and ground in a specific machine, then sieved and dried in an oven

at 103 ± 2˚C before characterization.

2.3.2. Preparation of the Clay

The preparation of the clay (Figure 2) makes it homogeneous and pure; it is dried (40˚C for 24 hours), crushed in an agate bowl, and sifted using a sieve to obtain a fine and homogeneous powder of less than 350 µm [17]. All this is to ensure the reliability, reproducibility, and representation of the intrinsic properties of the clay.

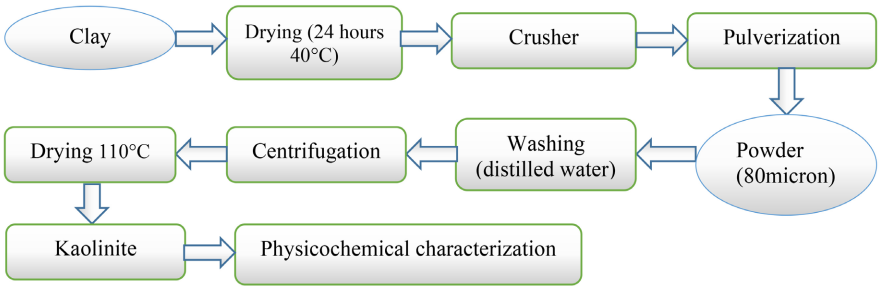

Figure 2. Clay preparation process.

2.4. Assembly of the Test Plan

Before any handling, a test board is set up using the Statgraphics 18.0 software as shown in (Table 1). A Simplex Centroid-type mixture design was carried out to optimize 3 experimental variables: clay (30 - 35), Ayous dust (30 - 35), and the binder (15 - 20) while keeping the water percentage constant (15%) throughout the experiment. The response for each of these tests is the density ρ_0 (g/cm^3). The optimization objective and the reason for choosing the 10 formulations lie in the fact that this method allows obtaining the maximum mathematical information with the minimum number of laboratory manipulations. Indeed, a test board is essential for the handling and characterization of composites because it allows controlled mechanical tests to evaluate the properties of the composite, such as tensile, bending, or shear testing. This is necessary to obtain usable results on the composites [18].

Table 1. Formulation test plan.

N˚	Code	Ayous sawdust	Clay	Binder	water	Total mass (g)
01	PA	35	35	15	15	199
02	PB	35	30	20	15	199
03	PC	30	35	20	15	199
04	PD	34.16	34.16	16.66	15	199
05	PE	34.16	31.66	19.16	15	199
06	PF	31.66	34.16	19.16	15	199
07	PG	35	32.5	17.5	15	199
08	PH	32.5	35	17.5	15	199
09	PI	32.5	32.5	20	15	199
10	PJ	33.33	33.33	18.33	15	199

2.5. Preparation of the Composite

The manufacturing process of the specimens shown in Figure 3 must be carried out carefully, following the previously established mixing plan (Table 1). Once the sawdust and wood are dried, proceed to the first mixing and stir dry with a mixer for approximately 4 minutes.

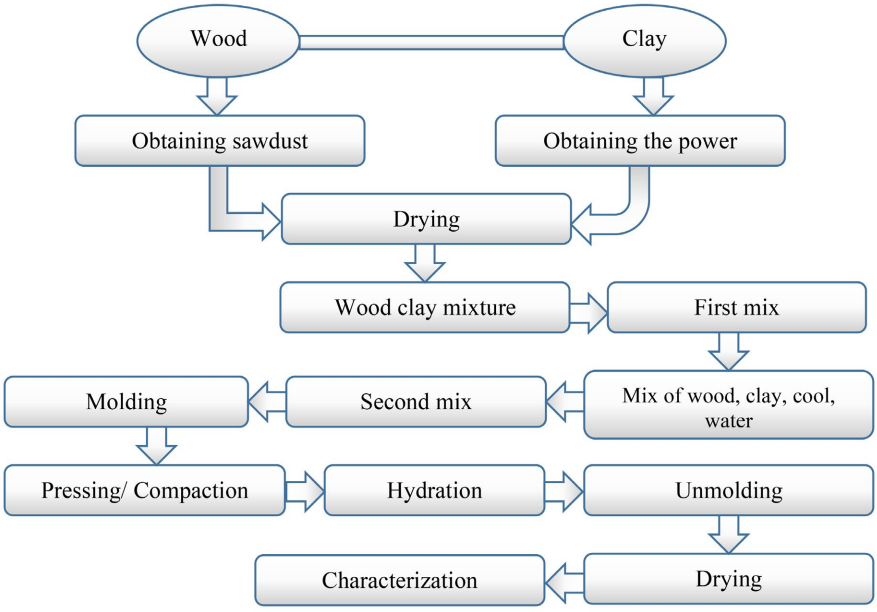

Figure 3. Composite preparation process diagram.

Prepare the wood vinyl glue, then take 15% water of the total mass of each specimen and proceed to the second mixing for about 8 to 10 minutes until it is homogeneous. Prepare the mold and cover it with plastic wrap to facilitate demolding of the specimens, then compact it using a mass with an average load of 5 MPa, let it hydrate for 24 hours, demold it, and air-dry for 18 hours, then dry it in an oven at 103˚C (±2) until its mass stabilizes [19]. For each formulation, three distinct specimens were independently prepared to ensure the reproducibility of results and to serve as independent biological and technical replicates.

Table 2. Manufacturing parameters for (wood-clay) specimens.

Parameter	Specifications/Values	Technical Observations
Matrix (Binder)	vinyl wood glue	Water-soluble, hardening by evaporation.
Mineral Filler	Mbalmayo clay	Local clay from the sedimentary basin of the Centre region.
Woody Reinforcement	Ayous sawdust (*Triplochiton scleroxylon*)	Low-density wood (0.35 to 0.45 g/cm^3).
Granulometry (G)	0.31 to 0.35 mm	Narrow granulometric range for homogeneity.

Continued

Mold Dimensions	**176.5 × 58.8 × 18.8 mm**	**Useful mold volume: ≈195.1 cm³.**
Target Thickness (h)	16 mm	Induces a compression rate of ≈15%.
Water Content ($\acute{\omega}$)	15%	Necessary balance for mixture processing.
Compaction Pressure	5 MPa	Moderate pressure for wood-clay composite.
Pressing Time	15 min	Shaping and initial cohesion phase.
Drying Protocol	18 days (30˚C) + Oven (103 ± 2˚C)	Slow drying (prevents cracks) followed by stabilization.

Table 2 below presents the development of a bio-sourced composite that combines the porosity of Ayous with the plasticity of Mbalmayo clay, stabilized by a vinyl adhesive to optimize interfacial adhesion. The protocol focuses on using a fine granulometry that increases the specific surface area and contact points, while compaction at 5 MPa under a 15% compression rate reduces inter-particle voids to enhance density and mechanical strength.

2.6. Physicho-Chemical Characterization Techniques

The surface morphological characteristics and the elemental composition of the materials were examined by the scanning electron microscopy (SEM) coupled with energy-dispersive X-ray spectroscopy (EDX) using a JEOL-JSM-6390A device (Tokyo, Japan) with an accelerating voltage of 10 kV and a magnification range of 25x to 1000 kx for this purpose. The crystallinity of the phases was determined by X-ray diffraction (XRD) using a PAN XPERT Pro powder X-ray diffractometer. The device was operated at 30 mA and 40 kV using Cu-K $\alpha 1$ radiation with a wavelength of 1.54056 Å at a scan rate of 5˚/min over a 2θ range of 10˚ to 90˚. The surface functional groups present in the materials are identified by Fourier-transform infrared spectroscopy (FT-IR) using a Nicolet IS5 Thermo Scientific spectrometer. The spectra were recorded in continuous mode between 4000 and 400 cm^{-1} by using the attenuated total reflection (ATR) technique. Once the IR radiation passed through the sample, a spectrum of the intensity of the radiation transmitted by the sample as a function of the wavenumber was recorded.

The Measurement Protocol

(Table 3) for the anhydrous density (ρ_0) of these composite specimens is based on ISO 13061-2 standard.

Required Equipment

- Thermostatic oven (105 - 110˚C).
- Precision balance (0.01 g).
- Vernier caliper or micrometer.

- Dehumidification ovens.

Table 3. Density measurement steps.

Step	Description	Duration/ Precision
1. Preparation	Clean and measure dimensions (L = 150 mm, l = 50 mm, e = 16 mm) of each specimen; calculate V = L × l × e (in m^3 or cm^3).	0.01 mm
2. Initial Weighing	Weigh the molded specimen (mf = 199 g) at ambient state.	0.01 g
3. Anhydrous Drying	Place in oven at 105 ± 2˚C until constant mass (loss <0.1% over 24 h); typically 24 - 48 h for wood composites.	Constant mass
4. Anhydrous Weighing	Cool 1h in desiccator, then weigh m_0 (dry mass).	0.01 g
5. Calculation	$\rho_0 = m_0/V$ (g/cm^3); error and uncertainty < 1%.	-

2.7. Mechanical Characterization in Three-Point Bending

The bending test was carried out in accordance with the normative reference EN 310 [20]. The cutting and sizing assigned to this test specimen are given by standards EN 325; EN 326-1, which are 150 mm × 50 mm × 16 mm. This European standard specifies a method for determining the apparent modulus of elasticity in axial bending and the bending strength of wood-based panels with a nominal thickness equal to or greater than 3 mm.

2.7.1. Principle

The process involves determining the flexural modulus (MPa) as well as the flexural strength by applying a force in the middle of a sample supported by two points. The slope of the linear portion of the load-deformation curve allows us to determine the modulus of elasticity: The determined value is the apparent modulus, which varies because the analysis method includes both shear and bending. The bending stress of each sample is calculated by taking the ratio of the bending moment M to the rupture load Fmax at the cross-section.

2.7.2. Equipment

The testing devices (Figure 4) below mainly consist of the following elements. The two cylindrical roller supports are placed parallel with a length greater than the width of the specimen and a diameter of d = (15 ± 0.5) mm; the distance between the supports is adjustable. An identical length for the cylindrical knife with a diameter of (30 ± 0.5) mm is placed parallel to the supports and at an equal distance, dimensions in millimeters.

The appropriate tool for measuring the deflection of the specimen at the center of the span with an accuracy of 0.1 mm; an analysis system to determine the load applied to the specimen with an accuracy of 1% of the obtained result.

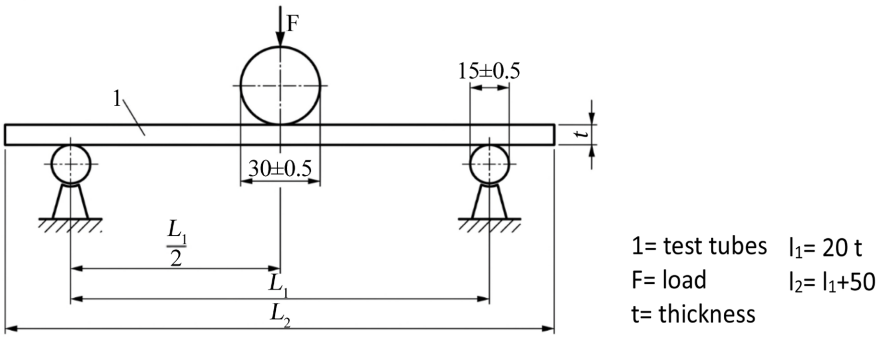

Figure 4. Bending testing device.

2.7.3. Flexural Modulus

The flexural modulus of elasticity E_m (in newtons per square millimeter) of each test specimen were calculated using the following formula:

$$E_m = \frac{l_1^3 (F_2 - F_1)}{4bt^3 (a_2 - a_1)}$$

For each set of test specimens, the flexural modulus taken from the same panel corresponds to the arithmetic mean, expressed with three significant figures, of the flexural moduli of the specimens considered.

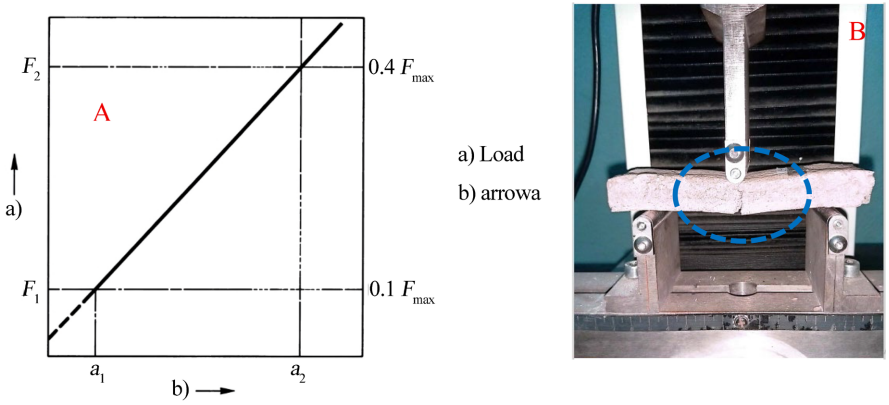

Figure 5. Load-deformation curve (elastic deformation domain) (a) and 03 point bending test showing the crack (b).

The three-point bending curve is presented in the form of force-displacement. The curve evolves through three phases before the appearance of the first crack (Figure 5(a)), as shown in (Figure 5(b)), corresponding to the response of the specimens.

Phase 1: The first stage describes the linear plastic behavior of the wood-clay material. During this period, the Young's modulus changes very little, and no impact is visible to the naked eye.

Phase 2: During the second stage, a nonlinear elastic behavior of the composite material is observed. It is characterized by a gradual decrease in the stiffness of the structure and in the Young's modulus.

Phase 3: This final stage occurs beyond the peak of the curve and indicates the failure point of the composite (composite cracking). The crack propagates and leads to total rupture [18].

2.7.4. Resistance to the Bending Test

The bending stress f_m (in Newtons per square millimeter) of the test specimens is calculated from the following formula:

$$f_m = \frac{3F_{\max} l_1}{2bt^2}$$

where: $F_{\max}$ = breaking load, in Newtons, l_1, b, and t are in millimeters.

According to ASTM D790 and ISO 178 standards, for a rectangular cross-section composite panel specimen (width b, thickness h), subjected to three-point bending with span length L, the maximum flexural stress is given by the following equation.

$$\sigma\_\max = 3FL/(2bh\,\hat{}\,2)$$

where:

- F is the applied force (in N),
- L is the span length between supports (in mm),
- b is the specimen width (in mm),
- h is the specimen thickness (in mm).

Regarding the elastic limit in flexure, on the force-deflection (or stress-deflection) diagram, identify the point where the curve deviates from the linear portion (onset of plastification or non-linearity). The corresponding force F_{elas} represents the force at the elastic limit in flexure. The elastic limit stress in flexure σ_{elas} is then given by:

$$\sigma\_elas = (3F\_elas\ L)/(2bh\,\hat{}\,2)$$

It is expressed in MPa (or N/mm^2) and is commonly used in flexural testing on composites (ASTM D790, ISO 178).

For each group of specimens, the bending strength taken from the same panel corresponds to the arithmetic mean expressed with three significant figures of the bending strengths of the specimens considered.

3. Results and Discussion

3.1. Characterization of Raw Materials

3.1.1. Analysis by XRD and FT-IR Spectroscopy of Kaolin and Wood Sawdust

The analysis of the clay X Ray diffractogram (**Figure 6**) reveals that the composition is dominated by quartz and kaolinite, with minor amounts of goethite and anatase. The results obtained are in agreement with those reported by [21] on the clays of Mbalmayo (central Cameroon).

The peaks present on the diffractogram (**Figure 6**) of Ayous wood sawdust are associated with planes attributed to the crystallographic plane of cellulose. The

peak at 14.9˚ is attributed to the crystallographic plane (110) and the one at 22.26˚ to the crystallographic plane (200) of cellulose according to [22]. These 2θ diffraction peaks reveal the native form of cellulose, characteristic of lignocellulosic materials, crystallographically of cellulose.

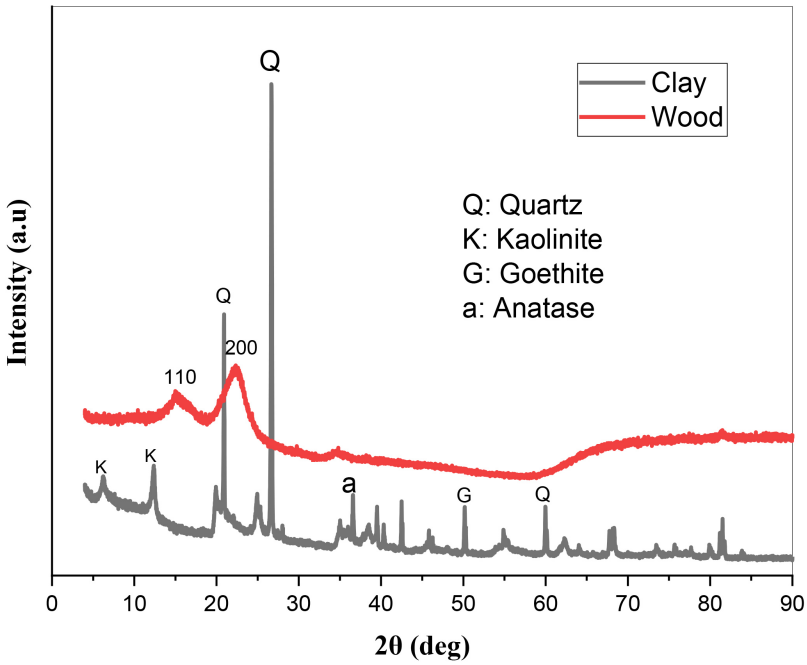

Figure 6. XRD Diffractogram of clay and Wood.

The examination of the IR absorption spectrum of kaolin (**Figure 7**) shows three bands between 4000 - 3500 cm^{-1}, which are attributable to the OH stretching vibration peaks of kaolinite [23]. The other bands at 1028 and 1005 cm^{-1} correspond to the (Si-O-Si) and Si-O-T where (T is Si or Al) bonds, respectively [24]; vibrations in the plane at 911 cm^{-1}, attributed to Al-OH bending vibration; 779, 751, 529 cm^{-1} symmetric and asymmetric vibrations of the Si-O-Al groups that characterize Kaolinite. The IR spectrum of kaolin does not show suitable bands for organic matter and carbonates, notably in the region 2954 - 2810 cm^{-1} and 1400 cm^{-1}, as their characteristic bands are not observed [25]. In the IR-TF spectrum of Ayous wood (**Figure 7**), the band at 3360 cm^{-1} in the absorption range corresponds to the stretching vibrations of the O-H bond. This indicates the presence of aromatic structures and phenolic and alcoholic compounds corresponding to lignin and cellulose. The band extending to 2903 cm^{-1} is attributed to C-H stretching. The band located between 1650 and 1504 cm^{-1} is attributed to benzene stretching vibrations related to aromatic groups. Additionally, the band at 1262 cm^{-1} is attributed to the C-O vibration of the methoxyl groups of lignin. The band at 1023 cm^{-1} corresponds to the stretching vibrations of the C-O and C-O-C bonds of cellulose, and the bands between 1025 - 1035 cm^{-1} correspond to the C-O-C deformation vibrations. These bands are consistent with those reported by [26].

The band at 896 cm^{-1} is associated with antisymmetric stretching in the pyranose ring phase of cellulose [27].

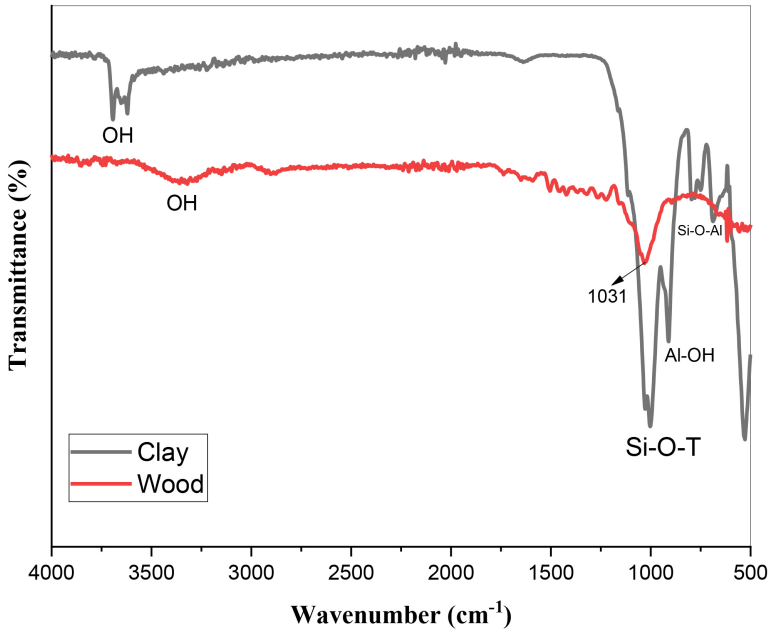

Figure 7. IR-TF Spectrum of clay and wood.

3.1.2. MEB Analysis of Kaolin and Ayous Wood Sawdust

Figure 8 shows the MEB analysis of clay (**Figure 8(a)**) and wood (**Figure 8(b)**). The image (**Figure 8(a)**) illustrates the morphology of the kaolin material; we can observe the particles arranged on either side with different shapes. It is also noted that its particles do not have a uniform coloration; nevertheless, the white color is dominant and similar to the kaolinite from Mayouom (western Cameroon) [28].

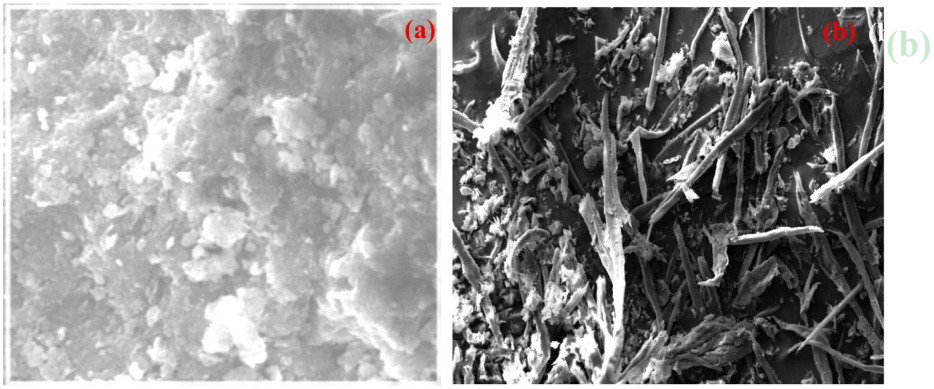

Figure 8. Morphology of clay (a) and wood (b).

This may be due to its elemental composition, as shown by spectral analysis and EDX. Direct observation of the ayous wood sawdust image (**Figure 8(b)**) shows a more or less irregular outer surface and a heterogeneous structure, similar to pine wood residues [29]. There is a noticeable color distinction, with white being dom-

inant in ayous sawdust due to its wood type, compared to sawdust from IROKO, DIBETOU, and MOABI, which are slightly darker [30]. The image shows scattered pores, which increase the material's absorption capacity. The photograph also reveals Fiber (microfibril) which is generally made of cellulose and lignin, constituting the main component of wood [31] [32]. Lignin provides rigidity to the cell wall [33].

3.1.3. EDX Analysis of Kaolin and Ayous Wood Sawdust

Figure 9 presents the EDX analysis of the clay (**Figure 9(a)**) and wood (**Figure 9(b)**). The EDX microanalysis of kaolin (**Figure 9(a)**) shows that it contains the elements oxygen (51.8%), sodium (0.5%), aluminum (16.7%), silicon (27.9%), potassium (0.8%), and iron (2.3%). However, the clay is rich in oxygen (51.8%), aluminum (16.7%), and silicon (27.9%) with a Si/Al ratio of 1.6; which is consistent with its use since the mechanical properties of clay-based geopolymers depend on alkalinity and the Si/Al ratio. It has been shown that a decrease in compressive strength is related to an increase in the Si/Al ratio to around 2.15. The slight increase in potassium content compared to sodium indicates that the breaking stress will be higher [34]. The EDX analysis (**Figure 9(b)**) of the Ayous sawdust material shows 67% oxygen (O), which is relatively higher than that reported in [29], at 40.6%. Indeed, oxygen is a major component of the functional groups present in the cellulose and lignin molecules of wood sawdust. The high oxygen content demonstrates that the material (wood sawdust) is largely composed of carbon- and oxygen-based organic compounds. The analysis records 9.5% silicon (Si), which is considered high for wood sawdust.

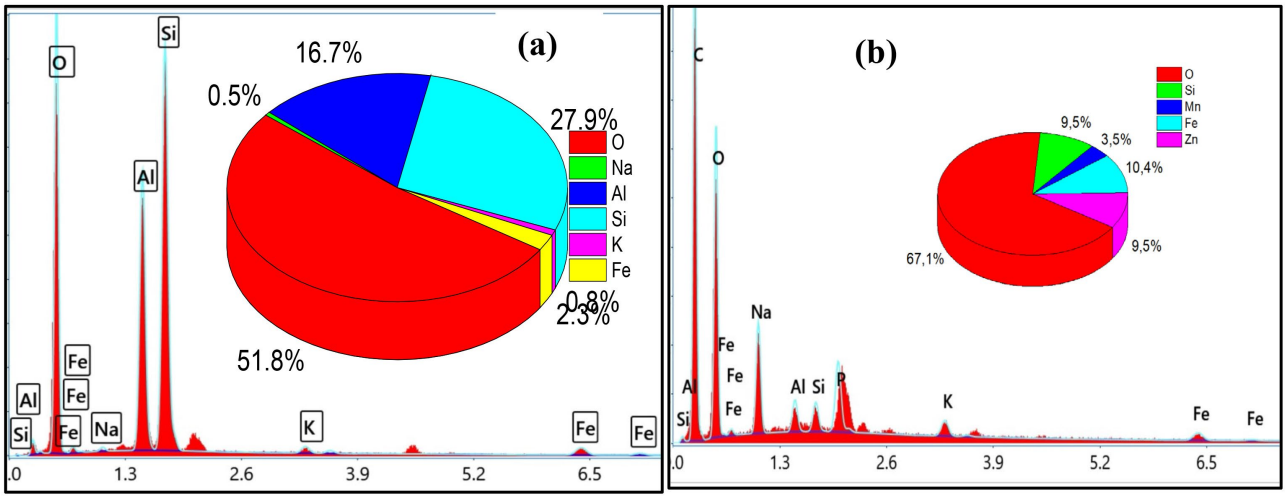

Figure 9. EDX of kaolin (a) and Ayous sawdust (b).

This could be due to contamination by mineral matter or inorganic elements from the manufacturing process or the soil. Furthermore, it indicates 10.4% manganese (Mn), which is relatively high for wood sawdust as an organic material and provides an advantage for the composite material because manganese enhances

the mechanical properties of the material. Furthermore, the presence of 9.5% zinc in Ayous wood sawdust is significant; it is used in treatment products for its ability to resist degradation and provide mechanical strength [35].

3.1.4. Data Analysis Formulation Test Plan

Table 4 under illustrates the relationship between the mixture compositions and the apparent density (ρ_0) of bio-composites based on Ayous wood and clay. Although the total mass (199 g) and water content (15%) were kept constant across all samples, slight fluctuations in density are observed, ranging from 1.38 to 1.41 g/cm^3. These minor variations indicate that volumetric substitution between wood sawdust (a lightweight material) and clay or binder (denser materials) influences the structural arrangement and internal porosity of the specimens during molding. The predominance of the 1.41 g/cm^3 value for several mixtures (notably PA, PC, PD, PF, PH, and PI) suggests a saturation threshold or compaction equilibrium for these specific proportions. Conversely, the reduction observed in sample PE (1.38 g/cm^3) may indicate an increase in void volume or less intense physico-chemical interactions between components, offering avenues for tailoring the final material's physical properties.

Table 4. Analysis formulation test plan.

N°	Code	Ayous sawdust	Clay	Binder	water	Total mass (g)	ρ_0 (g/cm^3)
01	PA	35	35	15	15	199	1.41
02	PB	35	30	20	15	199	1.40
03	PC	30	35	20	15	199	1.41
04	PD	34.16	34.16	16.66	15	199	1.41
05	PE	34.16	31.66	19.16	15	199	1.38
06	PF	31.66	34.16	19.16	15	199	1.41
07	PG	35	32.5	17.5	15	199	1.39
08	PH	32.5	35	17.5	15	199	1.41
09	PI	32.5	32.5	20	15	199	1.41
10	PJ	33.33	33.33	18.33	15	199	1.40

3.1.5. Mechanical Characterization Three-Point Bending Test

The bending test was carried out under 10 formulations, and each formulation contains 3 specimens, making a total of 30 samples analyzed in bending. The test was conducted at the CECAM laboratory at PK 10 in the city of Douala, Cameroon, in accordance with the EN 310 standard [20], using a universal testing machine with a 5 kN force sensor and at a constant speed of 1 mm/min. The mechanical properties evaluated in this study include the modulus of elasticity ML (MPa), the maximum static bending stress (σfmax), and the Young's modulus (E). The various stress-strain curves (**Figure 10**) allowed to analyze and derive **Table 5** using

Equations (1) and (2). This curve interpretation thus made it possible to obtain the exact values of the elastic limit (MPa), the maximum strength (MPa), and the Young's modulus (MPa).

Table 5. Interpretation of bending curves (Elastic limit, maximum resistance, young's modulus).

N°	Code	Ayous sawdust	Clay	Binder	Water	Elastic limit (Mpa)	Maximum strength (Mpa)	Young Module (Mpa)
01	PA	35	35	15	15	156.17 ± 7.33	254.77 ± 33.92	19.66 ± 0.08
02	PB	35	30	20	15	189.53 ± 26.03	213.63 ± 7.22	18.15 ± 1.59
03	PC	30	35	20	15	225.13 ± 62.63	254.93 ± 34.08	21.15 ± 1.41
04	PD	34.17	34.17	16.67	15	128.80 ± 34.70	168.23 ± 52.62	15.70 ± 3.04
05	PE	34.17	31.67	19.17	15	176.97 ± 13.47	215.40 ± 5.45	16.79 ± 2.95
06	PF	31.67	34.17	19.17	15	166.23 ± 2.73	194.50 ± 26.35	20.98 ± 1.24
07	PG	35	32.5	17.5	15	171.93 ± 8.43	207.40 ± 13.45	23.79 ± 4.05
08	PH	32.5	35	17.5	15	182.83 ± 19.33	269.47 ± 48.62	24.36 ± 4.62
09	PI	32.5	32.5	20	15	136.17 ± 27.33	196.97 ± 23.88	19.17 ± 0.57
10	PJ	33.33	33.33	18.33	15	101.20 ± 63.30	233.17 ± 12.32	17.63 ± 2.11

3.1.6. Comparative Analysis of the Different Flexural Strength Limits, Maximum Strengths of the Bending and Young's Moduli from Bending Tests of Specimens

By analyzing this data, it is clear that the PC (225.13 ± 62.63 MPa), PB (189.53 ± 26.03 MPa), and PH (182.83 ± 19.33 MPa) panels have the highest yield strengths, in that order (**Figure 10(a)**). This suggests that they are the most resistant to plastic deformation during the bending test. On the other hand, the PJ (101.2 ± 63.30 MPa), PI (136.16 ± 27.33 MPa), and PD (128.8 ± 34.70 MPa) specimens have lower yield strengths, which means they are less capable of withstanding bending stresses without undergoing permanent deformation.

The studied wood-fiber-reinforced polyethylene composites show a modulus of elasticity depending on the type of pine filler and particle size. This modulus ranges from 741 MPa to 832 MPa due to a 20% pine filler. Conversely, the CBP thermoplastic composite [36] exhibits a lower modulus of elasticity than the wood-kaolin composite.

The analysis of this data shows that the PH (269.46 ± 48.62 MPa), PC (254.93 ± 34.08 MPa), and PA (254.76 ± 33.92 MPa) specimens exhibit the highest maximum strengths, in that order (**Figure 10(b)**). These specimens are therefore the most capable of withstanding significant loads without breaking during the bending test. Conversely, the PD (168.23 ± 52.62 MPa), PF (194.5 ± 26.35 MPa), and PI (196.96 ± 23.88 MPa) specimens show lower maximum strengths, indicating that they are less capable of bearing high loads before breaking. The PB (213.63 ± 7.22 MPa), PE (215.4 ± 5.45 MPa), PJ (233.16 ± 12.32 MPa), and PG (207.4 ± 13.45 MPa) specimens fall within an average maximum strength range, with varied but relatively close performances.

The highest maximum strength is found in the PH panel (269.46 ± 48.62 MPa). The study conducted on the development of the Kaolin-glass fiber composite [37] reports maximum strengths according to the percentage of kaolin contained in the composite. We can note 60.55 MPa for pure glass fibers; 91.5 MPa with 30% kaolin; 110 MPa with 40% kaolin [37]. The maximum strength increases with a significant presence of kaolin in the glass fiber. Additionally, wood-clay composites (case study) behave similarly and have a greater maximum strength with a lower percentage than that of the kaolin-glass fiber composite.

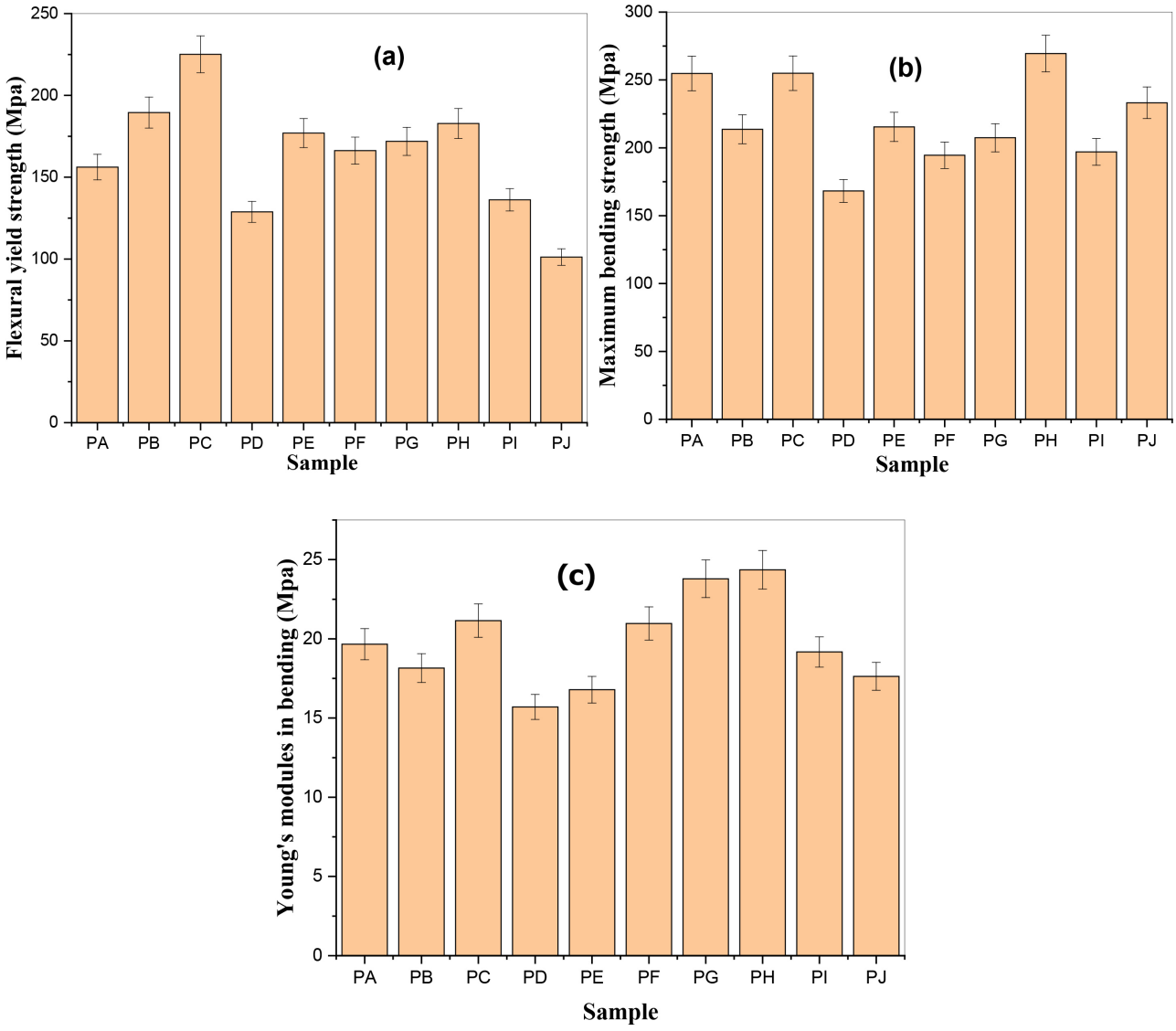

Figure 10. Flexural yield strength (a), maximum strengths of the bending (b) and Young's moduli from bending (c).

The PH specimen (24.36 MPa) presents the highest results. to resist bending while maintaining its stiffness (**Figure 10(c)**). In contrast, the PD specimen (15.70 ± 3.04 MPa) displays the lowest Young's modulus, indicating a lower ability to resist deformation under bending, while also showing reduced stiffness. The PC

(21.15 ± 1.41 MPa), PG (23.79 ± 4.05 MPa), PF (20.97 ± 1.24 MPa), PA (19.66 ± 0.08 MPa), and PI (19.16 ± 0.57 MPa) specimens exhibit almos similar performance in terms of Young's modulus, with intermediate values indicating good bending resistance and a certain level of stiffness. Finally, the PJ (17.63 ± 2.11 MPa), PB (18.15 ± 1.59 MPa), and PE (16.79 ± 2.95 MPa) specimens fall within a slightly lower range of Young's modulus compared to the previous specimens, meaning they offer slightly lower resistance and stiffness compared to the other specimens overall. We can say at the end of this analysis that the PH specimen (24.36 ± 4.62 MPa) presents the highest Young's modulus among all the specimens tested. The technical standard [38] EN 312 sets a minimum bending strength value of 11 N/mm^2 [39]. Studies carried out on date palms used for the production of wood panels and MDF report a bending stress on three wood species, namely: white wood (61.61 MPa); Dakar palm wood (13.73 MPa); and Ghers palm wood (13.75 MPa) [40]. In view of these results, a comparative analysis highlights a superior strength in favor of wood-kaolin composite materials, which exhibit a bending strength ranging between 19.16 MPa and 24.36 MPa. These results are consistent with the studies of [41]-[43].

Standard deviation analysis reveals significant structural disparity among the ten tested wood composite samples, highlighting variations in uniformity during flexural testing according to standards such as ASTM D1037 for modulus of elasticity (MOE) and maximum rupture strength (MOR). Samples PF (166.23 ± 2.73 MPa) and PG (171.93 ± 8.43 MPa) or PH (182.83 ± 19.33 MPa, depending on measurements) exhibit the lowest dispersions for the elastic limit (σ_e), demonstrating excellent mechanical repeatability and reliability, while PG and PH also dominate in stiffness with a Young's modulus (E) exceeding 23 MPa; conversely, PJ (101.20 ± 63.30 MPa) and PC (225.13 ± 62.63 MPa for elastic limit σ_e, coefficient of variation CV ≈ 28%) underscore instabilities due to production defects or granulometric variability, with CVs often > 25%. Overall, PH emerges as the optimal candidate for structural applications, offering superior maximum strength (269.47 ± 48.62 MPa), a robust Young's modulus (E = 24.36 ± 4.62 MPa), and moderate stability.

3.1.7. Bending Test Results with Other Composite Materials

The flexural test comparison table (**Table 6**) presents 5 results from the different components of the materials. The highest was obtained from Iroko wood composite with epoxy matrix (53.21 - 80.25 MPa). The second is the fiber particleboard made from collected anas, with a Young's modulus of 11.7 MPa. The materials with the lowest Young's modulus are those of date palm/polystyrene particles (0.12 - 0.76 MPa) and Gmelina wood (0.60 - 0.76 MPa).

Looking at all five materials presented in **Table 6**, it appears that the case study in this work (wood-kaolin composite) shows higher values (PH: 24.36 **±** 4.62 MPa) than the other four materials, except for the Iroko Wood composite with epoxy matrix. The results obtained are on average higher compared to those in the literature. The produced composites have better bending strength and can be

used in the construction and furniture industries. According to NF 312 standard, the produced composite belongs to type P2 panels (panels for interior fittings, including furniture, used in dry environments).

Table 6. Comparison of bending test results with other composite materials.

Composite		Young Module (Mpa)	Reference
Particle board containing plastic waste	PB	3.807 ± 0.85	[8]
	P10	5.582 ± 0.91	
	P15	5.540 ± 1.30	
	P20	5.429 ± 1.06	
	U10	5.380 ± 0.60	
	U15	5.605 ± 0.60	
	U20	6.746 ± 1.44	
Fiberboard panels from collected shives	RS	2.1 ± 0.7	[44]
	RSL	8.0 ± 1.2	
	ES	11.7 ± 0.8	
	HS	10.3 ± 1.7	
Date palm particles/polystyrene (PS)		0.12 à 0.76	[2]
Wood of Gmelina/PS		0.60 - 2.26	
Iroko wood composite with epoxy matrix		53.21 - 80.25	
Kaolin Wood composite	PA	19.66 ± 0.08	This study
	PB	18.15 ± 1.59	
	PC	21.15 ± 1.41	
	PD	15.70 ± 3.04	
	PE	16.79 ± 2.95	
	PF	20.98 ± 1.24	
	PG	23.79 ± 4.05	
	PH	24.36 ± 4.62	
	PI	19.17 ± 0.57	
	PJ	17.63 ± 2.11	

3.1.8. Curved Bending Stress-Strain Test

Figure 11 and Figure 12 below show the force-displacement stress curves obtained during three-point bending tests depending on the mixture percentage of the test plan (wood, clay, glue, water).

The analysis of the best results obtained among the 30 samples tested in the three-point bending test, as shown in the images above, highlights the following points: Yield strength (Figure 11): The PC specimens showed a yield strength of 225.13 MPa. This result represents the maximum stress that these samples can withstand before undergoing permanent plastic deformation. Such a value sug-

gests a good ability to resist elastic deformations under load. However, maximum bending strength (**Figure 11**): The PH specimens exhibited a maximum bending strength of 269.46 MPa. This value indicates the maximum load these samples can withstand before fracturing or breaking, demonstrating excellent bending resistance. Furthermore, this leads to the Young's Modulus (**Figure 11**): The Young's moduli of the PG and PH specimens are 23.79 MPa and 24.36 MPa, respectively. It measures the stiffness of the material. These values show that the PH specimens are slightly stiffer than the PG specimens, indicating their ability to deform elastically under applied stress. In conclusion, among the tested samples, the most notable results are: the PC specimens (**Figure 11**) for the highest yield strength at 225.13 MPa, and the PH specimens (**Figure 11**) for the highest flexural strength at 269.46 MPa, similar to [43] [44], and for the highest Young's modulus at 24.36 MPa. These results suggest that the PH specimens stand out particularly for their combination of stiffness and high flexural strength, while the PC specimens are distinguished by their higher yield strength among the samples studied. All this is due to a kaolin proportion roughly equal to that of the wood sawdust.

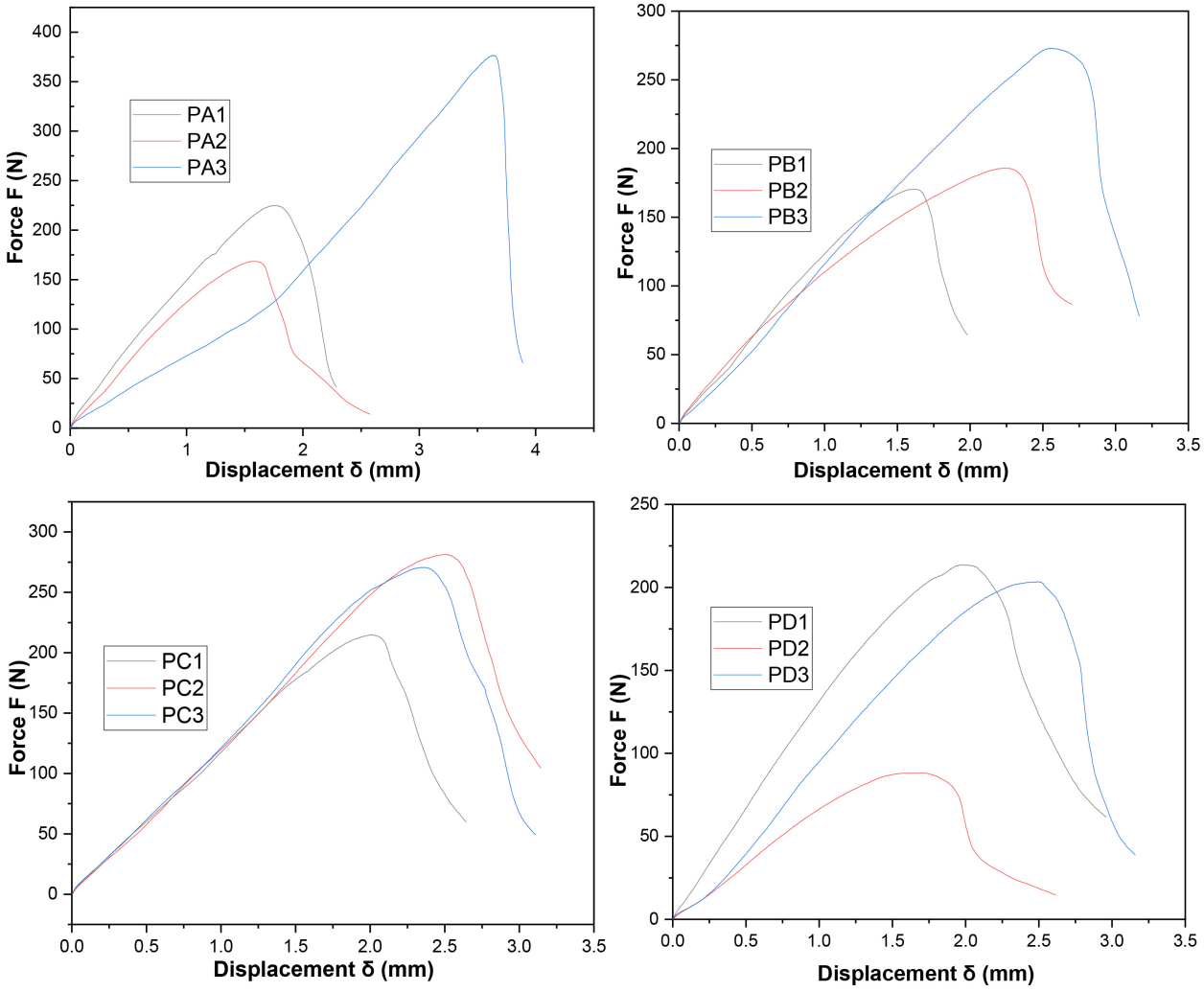

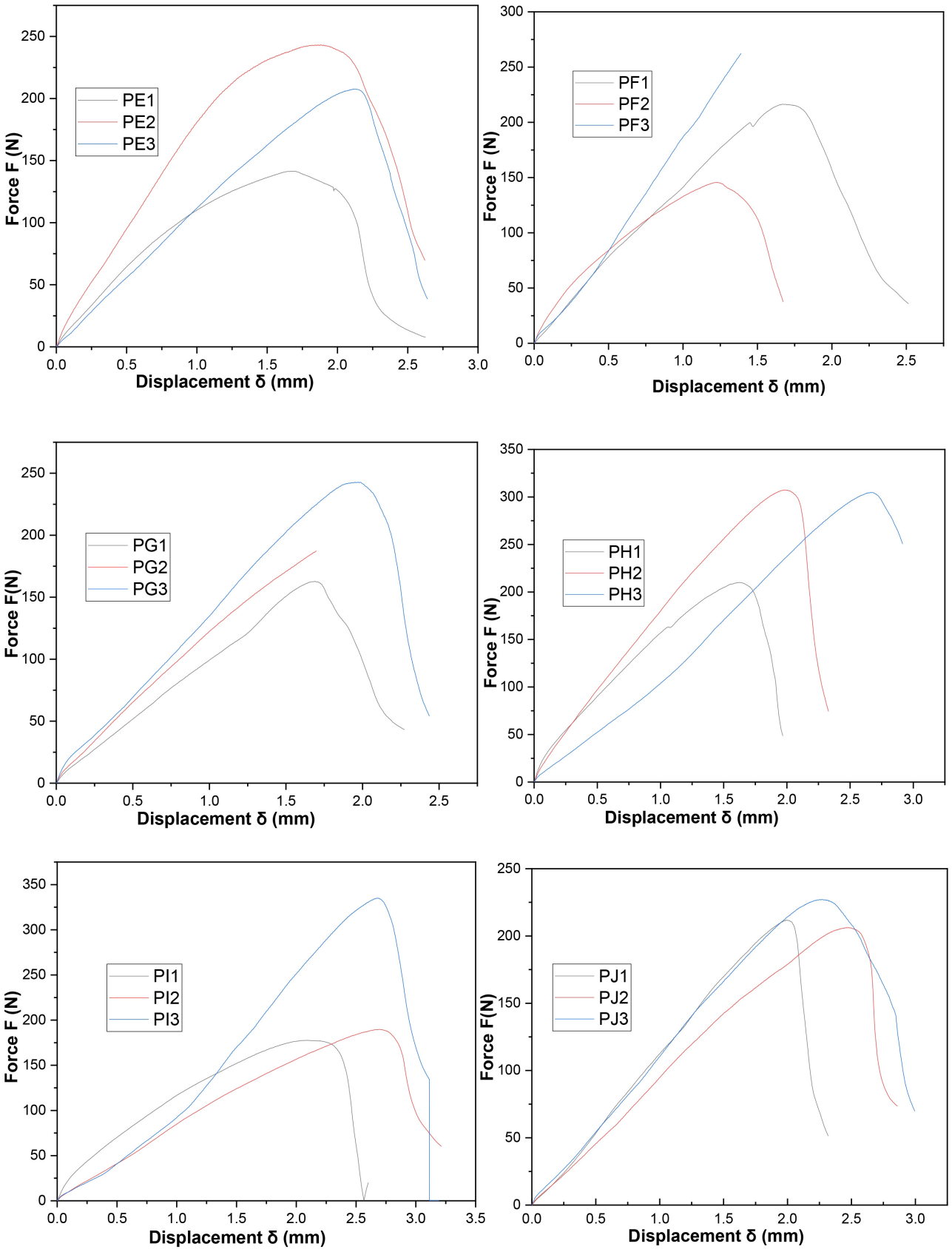

Figure 11. Bending stress-strain graph of different sample.

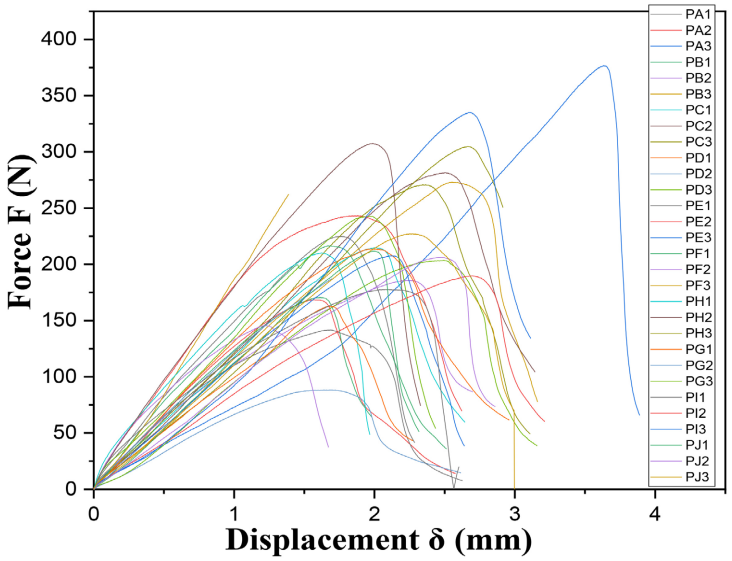

Figure 12. Constraints of the 30 stress curves deformation in bending.

3.2. Characterization of the Composite

Figure 13 presents the XRD, SEM, and EDX results of the composite. The EDX (**Figure 13(a)**) microanalysis of the wood-kaolin composite shows an elemental composition dominated by the clay matrix with contributions from the wood fibers. This composite indicates a strong presence of oxygen, silicon, aluminum, and carbon, reflecting the silicates of the clay and the organic compounds of the wood [45]-[47]. Iron, calcium, and titanium appear as trace elements from natural impurities [48]. The EDX spectra commonly identify in the wood-clay composite: Carbon (C) 31.4%, high due to the wood fibers [45] [46], and Oxygen (O) 38.5% as major components of the structure. Silicon (Si) 16.7% as components of the silica-alumina structure of the clay. Aluminum (Al) 9.9% from the aluminosilicates of the clay [48] [49]. Iron (Fe) 1.6%, Titanium (Ti) 1.1%, and Calcium (Ca) 0.7% as minor elements from soil or wood minerals [45] [48].

The in-depth analysis of the spectra allows us to draw conclusions that the moderate peaks of Si and Al confirm the persistence of kaolinitic or smectitic phases. The significant carbon signal, on the other hand, attests to the homogeneous integration of wood fibers within the structure. An O/Si atomic ratio greater than 2 suggests the presence of hydrated silicates. Furthermore, the low Ca content (0.7%) indicates a limited presence of carbonates [47] [50] [51]. A notable disappearance of potassium (K), initially present in raw kaolin, is observed, while titanium (Ti) remains detectable in the final composite. This modification may reflect the physicochemical interactions that occurred during the preparation of the mixture.

The microstructure of the wood sawdust-kaolin composite reveals a homogeneous matrix, free of excess woody fibers or prominent voids, indicating excellent dispersion and optimal interfacial affinity [45]-[47] The observed surface exhibits a compact texture, characterized by diffuse porosity composed of fine inter-fiber

pores. This structure is favored by the fine particle size of the sawdust (less than 0.3 mm) [46] [47]. Furthermore, the absence of interfacial porosity between the wood and kaolin confirms strong adhesion as well as a perfectly isotropic distribution of the phases [45] [47].

However, the XRD spectrum of the composite was also carried out to identify the mineral phases formed by the interaction between the kaolin and wood. **Figure 13(c)** shows that the composite retains the characteristic peaks of the starting clay with a predominantly amorphous structure, consisting of small peaks corresponding to kaolinite and quartz. The disappearance of the peaks located at 14.9˚ is attributed to the crystallographic plane (110) and the peak at 22.26˚ to the crystallographic plane (200) of cellulose, which can be attributed to the presence of an excessive amount of kaolin, exceeding the quantity necessary to capture the available cellulose [52].

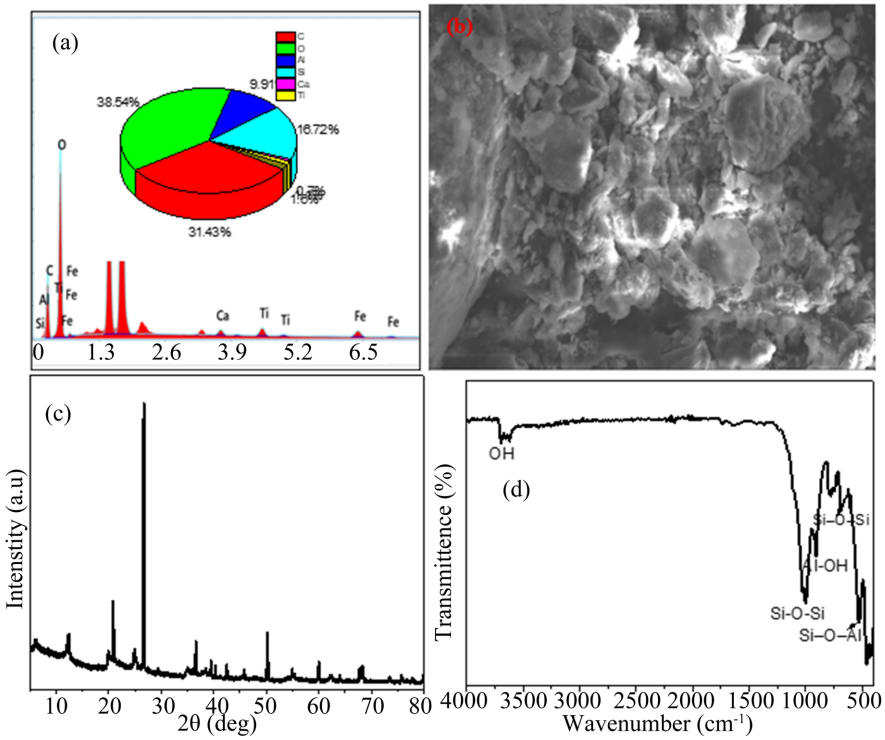

Figure 13. XRD (a); MEB (b); EDX (c) and FTIR (d) of composite after formulation.

The adjacent figure (**Figure 13(d)**) shows the characteristic FTIR bands of the composite obtained after formulation. Three bands are observed between 4000 - 3500 cm^{-1}, which are attributable to the OH stretching vibration peaks of kaolinite [53]. The bands at 1029 and 1003 cm^{-1} correspond respectively to (Si-O-Si) and Si-O bonds [54]; vibrations in the plane at 911 cm^{-1} are attributed to the Al-OH deformation vibration. Other bands at 691cm^{-1} were attributed to Si-O-Si deformation, and the one at 533 cm^{-1} to Si-O-Al deformation in kaolinite [55]. These bands are identical to those identified in the starting kaolin, which shows that the composite formulation did not completely modify the characteristic bands of ka-

olinite. However, no band corresponding to the valence vibrations of the C-O and C-O-C bonds of cellulose and the methoxyl groups of lignin, characteristic of the addition of wood in the composite, is observed. This weak, undetectable band of ayous sawdust in the composite can be explained by chemical degradation during drying and spectral overlap. This result is consistent with those observed in the XRD analysis of the composite.

4. Conclusion

The insufficient processing of wood waste (30% to 36%) in Cameroon prompted us to work on the production of composite panels using sawdust residues from Ayous wood (Triplochiton chleroxylon) from a sawmill in Bondje, located in Eastern Cameroon in the Yokadouma district of the Boumba and Ngoko department; with a sieve size between (0.31 - 0.35 µm), the results were therefore appreciable. The clay matrix was collected in Mbalmayo near the Nyong River in the Nyong-et-So'o department of the Central region of Cameroon. This innovative mixing of renewable and mineral raw materials generates interest in meeting sustainability requirements. Furthermore, it is with this in mind that this study proposes an in-depth analysis of the production and characterization of the physicochemical properties and mechanics of this unique composite. After the test panels were completed, the surface morphology and elemental composition of the materials were analyzed by scanning electron microscopy (SEM), followed by mechanical characterization through a bending test in accordance with the EN 310 standard. The results obtained were compared with certain literature values, including the breaking stress (MPa) and Young's modulus (MPa), which allowed the determination of its application domain as type 02; to be used in dry environments and a humid area as indicated by the EN 312 standard. The results obtained during this work open up inventive prospects for the use of this interesting composite material in various industrial applications, while also leaving room for improvements to optimize their mechanical performance.

Acknowledgements

The authors are thankful to all members of the Research Team of the University of Douala, Cameroon, and also Mr LENOU Idriss for his contribution and also grateful for the "Allocation spéciale pour la modernisation de la recherche universitaire" from the Ministry of Higher Education (Cameroon).

Consent for Publication

All the authors consent to publication.

Conflicts of Interest

The authors declare no conflicts of interest regarding financing, experimentations and writing of the manuscript of this work.

References

[1] Amadji, T.A., Adjovi, E.C., Gérard, J., Barés, J. and Huon, V. (2021) Étude des propriétés technologiques d'un composite bois-plastique élaboré au Bénin. *BOIS & FORETS DES TROPIQUES*, **348**, 49-63. https://doi.org/10.19182/bft2021.348.a36750

[2] Takoumbe, C., Zobo Mfomo, J., Biwole, A.B., Mbou Tiaya, E., Mono, J.A., Pokem Nguimjeu, P.H., *et al.* (2024) Effect of Reinforcement Ratio and Particle Size on the Physical and Mechanical Performance of Epoxy Matrix Panels and Waste Wood from Iroko Chlorophora Excelsa from Cameroon. *Advances in Materials Science and Engineering*, **2024**, Article ID: 9915731. https://doi.org/10.1155/2024/9915731

[3] Groutel, E. (2021) Prospective on the Timber Industry by 2050: The Vision of Students from the School of Wood. 557-563. https://hal.science/hal-03447352v1

[4] Drovou, S., Assogba, K.K. and Sanda, K. (2015) Development and Mechanical and Physical Characterization of Particleboards Made from Kapok Sawdust with Tannin Powder from the Pod Husk of Nere. *European Scientific Journal*, **11**, 169-178.

[5] Celzard, A. and Leban, J. (2013) De nouveaux matériaux à base de bois: Un contexte, des exemples. *Revue Forestière Française*, **65**, 463-478. https://doi.org/10.4267/2042/53708

[6] Vernay, M. (2005) Un exemple d'utilisation de l'ayous (*Triplochiton scleroxylon*) dans la construction. *BOIS & FORETS DES TROPIQUES*, **284**, 35-43. https://doi.org/10.19182/bft2005.284.a20280

[7] Mahfoudh, A. (2013) Etude de la production et de la caractérisation de composites bois-plastiques. https://api.semanticscholar.org/CorpusID:139765592

[8] Mancel, V., Krilek, J., Čabalová, I., Réh, R., Osvaldová, M. and Darabošová, A. (2024) Evaluation of Selected Mechanical and Physical Properties of Particleboards Containing Waste Plastics. *Wood Research*, **69**, 169-178. https://doi.org/10.37763/wr.1336-4561/69.1.169178

[9] Slama, I. (2008) Physico-Mechanical Characteristics of Wood-Plastic Composites from the Valorization of MDF Panel Residues: study of Recycling Possibilities. Doctoral Thesis. University of Quebec in Abitibi-Témiscamingue. https://depositum.uqat.ca/id/eprint/22

[10] Nghueo Yemele, M. (2008) Development of Particle Boards on Black Spruce Bark and Aspen Poplar. Ph.D. Thesis, Université Laval.

[11] Gwon, J.G., Lee, S.Y., Chun, S.J., Doh, G.H. and Kim, J.H. (2011) Physical and Mechanical Properties of Wood-Plastic Composites Hybridized with Inorganic Fillers. *Journal of Composite Materials*, **46**, 301-309. https://doi.org/10.1177/0021998311413690

[12] Çelik, D.N. and Durmuş, G. (2022) The Development of Ultralightweight Expanded Perlite-Based Thermal Insulation Panel Using Alkali Activator Solution. *Frontiers of Structural and Civil Engineering*, **16**, 1486-1499. https://doi.org/10.1007/s11709-022-0881-6

[13] Peng, C., Kim, Y.J. and Zhang, J. (2021) Thermal and Energy Characteristics of Composite Structural Insulated Panels Consisting of Glass Fiber Reinforced Polymer and Cementitious Materials. *Journal of Building Engineering*, **43**, Article ID: 102483. https://doi.org/10.1016/j.jobe.2021.102483

[14] Reddy, J.R.T., Schuster, J. and Shaik, Y.P. (2024) Development of Kaolin and Glass Fiber Reinforced Composites for Thermal Insulating Panels. *Open Journal of Composite Materials*, **14**, 44-59. https://doi.org/10.4236/ojcm.2024.141004

[15] Nguyen, D.L., Luedtke, J., Nopens, M. and Krause, A. (2023) Production of Wood-Based Panel from Recycled Wood Resource: A Literature Review. *European Journal of Wood and Wood Products*, **81**, 557-570. https://doi.org/10.1007/s00107-023-01937-4

[16] Nkalih Mefire, A., Yongue Fouateu, R., Njoya, A., Mache, J.R., Pilate, P., Hatert, F., *et al.* (2018) Mineralogy and Geochemical Features of Foumban Clay Deposits (West Cameroon): Genesis and Potential Applications. *Clay Minerals*, **53**, 431-445. https://doi.org/10.1180/clm.2018.31

[17] Peck, D. (2001) Guide pour la réalisation et l'exploitation de planches d'essai sur DEG. Comité Français de Géosynthétique.

[18] Clément, L., Myriam, L.C., Pilar, F. and Olivier, S. (2020) Guide de solutions de séchage du bois buche. ADEME.

[19] Gizard, M. (2023) Suivi des travaux normatifs de la révision de la série des normes NF EN 12369 et de la norme NF EN 1058. FCBA.

[20] Mapuna, E.C.N., Aye, B.A., Ntouala, R.F.D., Ndjigui, P. and Bilong, P. (2023) Mineralogical, Geochemical, and Physicomechanical Features of the Mbalmayo Lateritic Clays (Southern Cameroon) for Potential Use as Raw Materials in the Making of Fired Bricks. *Arabian Journal of Geosciences*, **16**, Article No. 671. https://doi.org/10.1007/s12517-023-11791-6

[21] Kamgang Djioko, F.H., Fotsop, C.G., Kamgang Youbi, G., Nwanonenyi, S.C., Oguzie, E.E. and Ada Madu, C. (2024) Efficient Removal of Pharmaceutical Contaminant in Wastewater Using Low-Cost Zeolite 4A Derived from Kaolin: Experimental and Theoretical Studies. *Materials Chemistry and Physics*, **315**, Article ID: 128994. https://doi.org/10.1016/j.matchemphys.2024.128994

[22] Foko, R.U.N., Fotsop, C.G., Tchuifon, D.R.T., Banenzoué, C. and Azebaze, A.G.B. (2025) Green Synthesis of Magnetic Type Zeolites 4A as Catalyst for the Elimination of Quinoline Yellow by the Fenton Process: Optimization and Kinetic Investigation. *Hybrid Advances*, **9**, Article ID: 100401. https://doi.org/10.1016/j.hybadv.2025.100401

[23] Irfan Khan, M., Khan, H.U., Azizli, K., Sufian, S., Man, Z., Siyal, A.A., *et al.* (2017) The Pyrolysis Kinetics of the Conversion of Malaysian Kaolin to Metakaolin. *Applied Clay Science*, **146**, 152-161. https://doi.org/10.1016/j.clay.2017.05.017

[24] Poletto, M., Zattera, A.J., Forte, M.M.C. and Santana, R.M.C. (2012) Thermal Decomposition of Wood: Influence of Wood Components and Cellulose Crystallite Size. *Bioresource Technology*, **109**, 148-153. https://doi.org/10.1016/j.biortech.2011.11.122

[25] Esteves, B., Velez Marques, A., Domingos, I. and Pereira, H. (2014) Chemical Changes of Heat Treated Pine and Eucalypt Wood Monitored by FTIR. *Maderas. Ciencia y Tecnología*, **15**, 245-258. https://doi.org/10.4067/s0718-221x2013005000020

[26] Thakur, M., Sharma, A., Ahlawat, V., Bhattacharya, M. and Goswami, S. (2020) Process Optimization for the Production of Cellulose Nanocrystals from Rice Straw Derived α-Cellulose. *Materials Science for Energy Technologies*, **3**, 328-334. https://doi.org/10.1016/j.mset.2019.12.005

[27] Njoya, A., Nkoumbou, C., Grosbois, C., Njopwouo, D., Njoya, D., Courtinnomade, A., *et al.* (2006) Genesis of Mayouom Kaolin Deposit (Western Cameroon). *Applied Clay Science*, **32**, 125-140. https://doi.org/10.1016/j.clay.2005.11.005

[28] Caractérisation de la microstructure de sciure de bois de pin sylvestre Pinus sylvestris

[Microstructure Characterization of Scots Pine Pinus Sylvestris Sawdust]. *Journal of Materials and Environmental Science*, **6**, 765-772.

[29] Nko'o Abuiboto, M.C., Avom, J. and Mpon, R. (2016) Évaluation des propriétés de charbons actifs de résidus de Moabi (Baillonella toxisperma Pierre) par adsorption d'iode en solution aqueuse. *Revue des sciences de l'eau*, **29**, 51-60. https://doi.org/10.7202/1035716ar

[30] Perré, P. and Badel, É. (2006) De l'eau dans l'arbre à l'eau dans le matériau bois: Une introduction. *Revue Forestière Française*, **58**, 304-315. https://doi.org/10.4267/2042/6701

[31] Wertz, J. (2011) Les hémicelluloses: Note de synthèse. Document ValBiom-Gembloux Agro-Biotech, Université de Liège.

[32] Jarriault, A. (2015) Extraction of Hemicellulose from Paper Pulp for the Production of Dissolving Pulp. Ph.D. Thesis, Grenoble Alpes University.

[33] Selmani, S. (2020) Formulation of Aluminosilicate Binders from Different Tunisian Clays. Doctoral Thesis. University of Limoges; University of Sfax (Tunisia).

[34] Soini, S.A., Lalani, I., Maron, M.L., Gonzalez, D., Mahfuz, H., Domingo-Marimon, N., *et al.* (2025) Multiscale Mechanical Characterization of Mineral-Reinforced Wood Cell Walls. *ACS Applied Materials & Interfaces*, **17**, 18887-18896. https://doi.org/10.1021/acsami.4c22384

[35] Julson, J.L., Subbarao, G., Stokke, D.D., Gieselman, H.H. and Muthukumarappan, K. (2004) Mechanical Properties of Biorenewable Fiber/Plastic Composites. *Journal of Applied Polymer Science*, **93**, 2484-2493. https://doi.org/10.1002/app.20823

[36] Slama, I. (2008) Physico-Mécanical Characterization of Wood-Plastic Composites from MDF Panel Residues: Study of Recycling Possibilities. Doctoral Dissertation, University of Quebec in Abitibi-Témiscamingue.

[37] (2010) EN 312: Panneaux de particules—Spécifications. Comité européen de normalisation (CEN).

[38] Réh, D.H.R. (2024) Propriétés des panneaux de particules fabriqués à partir du recyclage des déchets municipaux et particules de bois. *ACTA Facultatis Xylologiae Zvolen*, **66**, 33-46.

[39] Bekkari, O. and Ayache, R. (2023) Production of MDF Wood Panels Based on Date Palm By-Products. Master's Thesis, Kasdi Merbah Ouargla University.

[40] Pędzik, M., Janiszewska, D. and Rogoziński, T. (2021) Alternative Lignocellulosic Raw Materials in Particleboard Production: A Review. *Culture and Industrial Products*, **174**, Article ID: 114162.

[41] Ihnát, V., Lübke, H., Russ, A. and Borůvka, V. (2017) Waste Agglomerated Wood Materials as a Secondary Raw Material for Chipboards and Fibreboards Part I. Preparation and Characterization of Wood Chips in Terms of Their Reuse. *Wood Research*, **62**, 45-56.

[42] Evon, P., Barthod-Malat, B., Grégoire, M., Medina, G.V., Labonne, L., *et al.* (2019) Production of Fiberboards from Shives Collected after Continuous Fiber Mechanical Extraction from Oleaginous Flax. *Journal of Natural Fibers*, **16**, 453-469.

[43] Risson, T. (1998) Creep Response of Neat and Carbon-Fiber-Reinforced PEEK and Epoxy Determined Using a Micromechanical Model. *Symmetry*, **12**, 1680. https://doi.org/10.3390/sym12101680

[44] Shi, J., Zhang, H., Liu, Y., Xia, C. and Zhang, Y. (2022) Induced Wood-Inorganic Composites in Standing Trees via Slow-Release Drip. *Polymers*, **14**, 3103.

https://doi.org/10.3390/polym14153103

[45] TESCAN Analytics (2024) SEM/FIB/EDX for Construction Materials. TESCAN Technical Site. https://www.tescan-analytics.com/Vos-applications/Vos-thematiques/Materiaux-de-construction-et-genie-civile-1

[46] Folorunso, D.O., Olubambi, P. and Borode, J.O. (2014) Characterization and Qualitative Analysis of Some Nigerian Clay Deposits for Rafractory Applications. *IOSR Journal of Applied Chemistry*, **7**, 40-47. https://doi.org/10.9790/5736-7914047

[47] Rallet, D., Paltahe, A., Tsamo, C. and Loura, B. (2022) Synthesis of Clay-Biochar Composite for Glyphosate Removal from Aqueous Solution. *Heliyon*, **8**, e09112. https://doi.org/10.1016/j.heliyon.2022.e09112

[48] Elghareb, A. (2001) Deterioration and Consolidation of Some Pottery Vessels in Tel Ajrud, Suez, Egypt. *International Journal of Conservation Science*, **10**, 415-428.

[49] Batır, O., Selçuk, N. and Kulah, G. (2017) Investigation of the Effect of Kaolin Addition on Alkali Capture Capability during Combustion of Olive Residue. *Combustion Science and Technology*, **191**, 43-53. https://doi.org/10.1080/00102202.2018.1452376

[50] Dahmani, F. And Laiche, D. (2020) Matériaux composite Argile-polysaccharide: Valorisation de ressources naturelles. Thèse de Doctorat. Université ibn khaldoun-tiaret.

[51] Hietz, P., Horsky, M., Prohaska, T., Lang, I. and Grabner, M. (2014) High-Resolution Densitometry and Elemental Analysis of Tropical Wood. *Trees*, **29**, 487-497. https://doi.org/10.1007/s00468-014-1126-7

[52] Ju, X., Bowden, M., Brown, E.E. and Zhang, X. (2015) An Improved X-Ray Diffraction Method for Cellulose Crystallinity Measurement. *Carbohydrate Polymers*, **123**, 476-481. https://doi.org/10.1016/j.carbpol.2014.12.071

[53] Drits, V.A., Zviagina, B.B., Sakharov, B.A., Dorzhieva, O.V. and Savichev, A.T. (2021) New Insight into the Relationships between Structural and FTIR Spectroscopic Features of Kaolinites. *Clays and Clay Minerals*, **69**, 366-388. https://doi.org/10.1007/s42860-021-00133-w

[54] Foroughi, M., Peighambardoust, S.J., Ramavandi, B. and Boffito, D.C. (2024) Simultaneous Anionic Dyes Degradation via H_2O_2 Activation Using Zeolite 4A/ZnO/$Fe_2(MoO_4)_3$ Nanoparticles in a Sono-Photocatalytic Process. *Advanced Powder Technology*, **35**, Article ID: 104320. https://doi.org/10.1016/j.apt.2023.104320

[55] Silva, F.A.N.G., Barbato, C.N., de Lemos Novo, B., Assis, T.C., Sampaio, J.A., Medeiros, M.E. and dos Santos Garrido, F.M. (2026) Reactive Silica Reduction in Brazilian Bauxite via Selective Grinding: Mineralogical and Physicochemical Insights into Kaolinite Behavior. https://doi.org/10.21203/rs.3.rs-7862142/v1